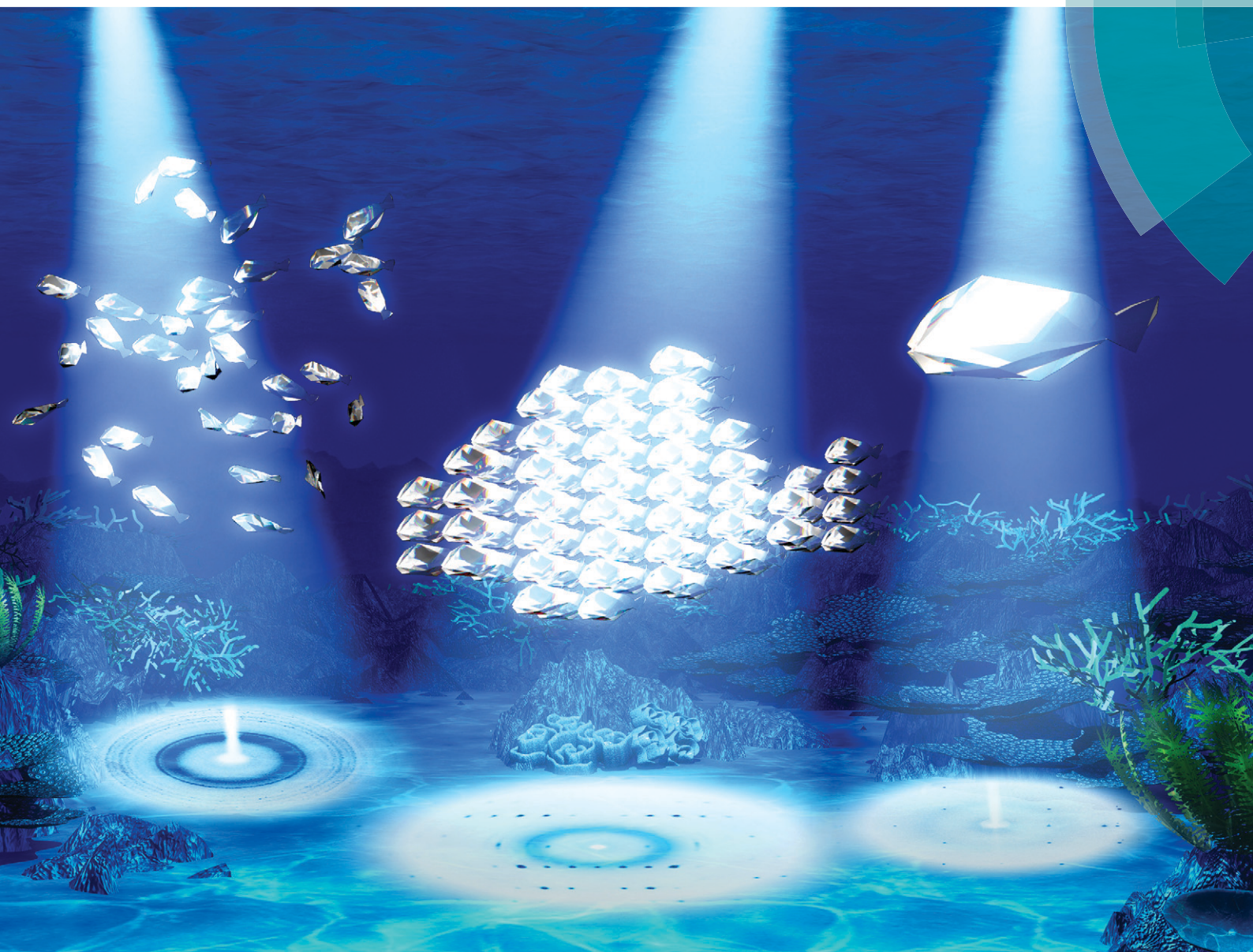# CrystEngComm

ROYAL SOCIETY
OF CHEMISTRY

COMMUNICATION
Tsunehisa Kimura *et al.*
Single-crystal structure determination from microcrystalline powders
(~5 μm) by an orientation attachment mountable on an in-house
X-ray diffractometer

175 YEARS

Single-crystal structure determination from microcrystalline powders (∼5 μm) by an orientation attachment mountable on an in-house X-ray diffractometer†

Chiaki Tsuboi,[a] Kazuaki Aburaya,[b] Fumiko Kimura,[a] Masataka Maeyama[b] and Tsunehisa Kimura*[a]

An X-ray attachment that can realize single-crystal X-ray diffraction patterns from microcrystalline powders is proposed. Single-crystal diffraction data are acquired *in situ* and analyzed using conventional computer software to determine the crystal structure of the microcrystals. The performance of the attachment is demonstrated using L-alanine microcrystals (∼5 μm).

The demand for single-crystal analyses has been increasing because the elucidation of molecular structures in crystalline states is of primary importance to understand and improve the functions and performance of solid materials in their final products. Single-crystal X-ray[1] and neutron diffraction techniques[2,3] are the most straightforward means to determine molecular structures if large single crystals are available. However, many materials are only available as microcrystalline powders that are unsuitable for characterization by these techniques. In such cases, powder diffraction is useful. The powder diffraction method has been rapidly and intensively developed recently.[4–12] However, it has substantial difficulties that the overlap of peaks is inevitable. Also, it strongly relies on model structure and computational optimization.

The overlap of peaks may be largely reduced if microcrystals are textured or partially oriented. Shape anisotropy of crystals was utilized for this purpose and single-crystal-like diffraction was successfully obtained to determine the crystal sturucture.[13–15] Liquid-crystals of a fibrous protein were magnetically oriented to obtain the fiber diffraction pattern for crystal structure determination.[16,17]

We previously proposed an approach to determine crystal structures from microcrystalline powders based on the three-dimensional (3D) magnetic orientation of microcrystals. This approach can be applied to biaxial crystals, including orthorhombic, monoclinic, and triclinic crystals, whose magnetic susceptibility tensor χ has three different principal values, χ_1, χ_2, and χ_3 ($\chi_1 > \chi_2 > \chi_3$). By applying frequency-modulated rotating magnetic fields to a suspension of microcrystals, the microcrystals are aligned three-dimensionally.[18,19] The χ_1 and χ_3 axes are referred to as easy and hard magnetization axes, respectively. The easy axis aligns parallel to the applied static field, while the hard axis aligns parallel to the rotating axis of the magnetic field. The combination of these two magnetic fields can produce 3D alignment of microcrystals. In actual experiments, the suspension is rotated in static magnetic fields instead of applying rotating magnetic fields.

In our approach, microcrystals suspended in a liquid medium are rotated with the rotating speed being changed regularly under a static magnetic field to achieve 3D alignment, and then the liquid medium is consolidated to fix the alignment of the microcrystals. The obtained composite, which is called a magnetically oriented microcrystal array (MOMA), produces X-ray diffraction (XRD) spots equivalent to those from a corresponding large single crystal. We have performed single-crystal X-ray analyses of MOMAs of inorganic, organic and protein microcrystal samples, and successfully solved their crystal structures.[20] However, it requires high magnetic fields (∼10 T) that are supplied by superconducting magnets in order to prepare MOMAs.

In this work, we design a compact orientation attachment, comprising a magnetic unit and shutter that can be mounted on an in-house X-ray diffractometer to obtain single-crystal XRD images from magnetically oriented microcrystal suspensions (referred to as MOMSs). *In situ* diffraction measurements from magnetically oriented suspensions are reported.[21–23] A schematic and photograph of the attachment are shown in Fig. 1. The directions of the impinging X-ray beam, magnetic field *B*, and rotation axis of the capillary

a Division of Forest and Biomaterials Science, Kyoto University, Sakyo-ku, Kyoto 606-8502, Japan. E-mail: tkimura@kais.kyoto-u.ac.jp; Fax: +81 75 753 6300; Tel: +81 75 753 6246
b Rigaku Corporation, 3-9-12 Matsubara-cho, Akishima, Tokyo 196-8666, Japan
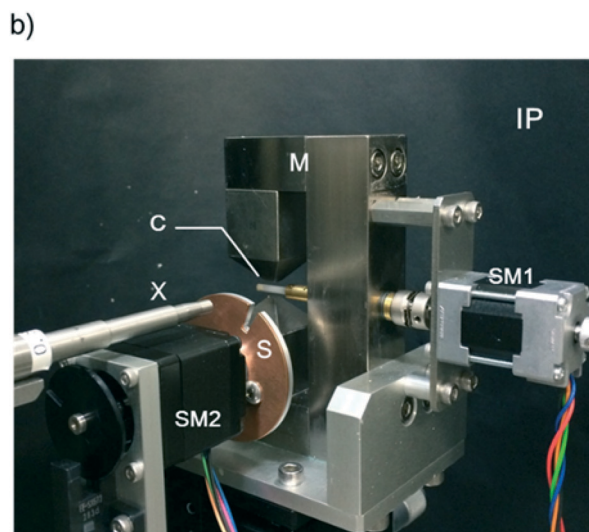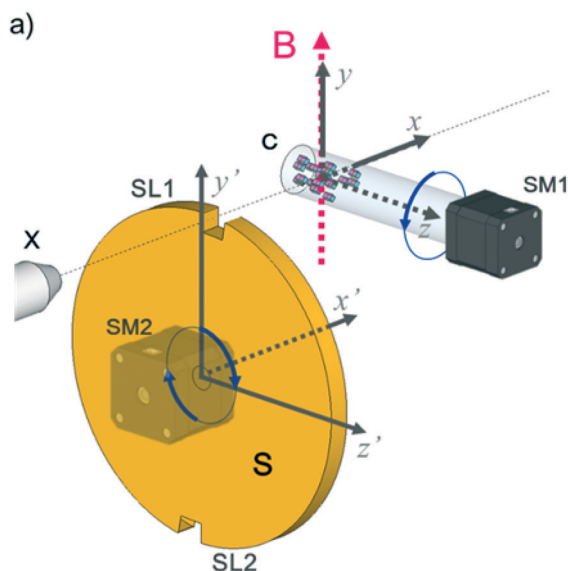
Fig. 1 (a) Schematic of the experimental setup. A glass capillary (C) containing a microcrystalline suspension rotates in a frequency-modulated manner by using a stepping motor (SM1) about the laboratory z axis under a static magnetic field (B). The x and y axes coincide with the directions of the impinging X-ray from a collimator (X) and the static magnetic field (B), respectively. The x', y', and z' axes, which are parallel to the x, y, and z axes, respectively, are the coordinates defined for the shutter (S) that has two slits (SL1 and SL2). The shutter is rotated synchronously with the capillary using a stepping motor (SM2). (b) Photograph of the orientation attachment mounted on an in-house X-ray diffractometer, where $\chi\phi$ goniometers are removed. This photograph shows a glass capillary (C), an X-ray collimator (X), stepping motors (SM1 and SM2), a shutter with a diameter of 44 mm (S), and a pair of neodymium magnets (M) generating *ca.* 1 T at the capillary. An imaging plate (IP) is at the back.
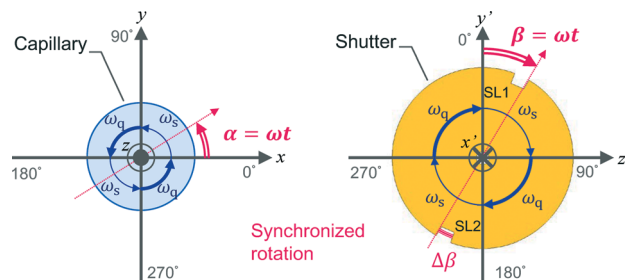

Fig. 2 Schematics of the rotation of the capillary and shutter. The xyz and x' y' z' coordinates are the same as in Fig. 1. The rotation angles $\alpha = \omega t$ of the capillary and $\beta = \omega t$ of the shutter are defined with respect to the x and y' axes, respectively. The rotation speed is $\omega = \omega_s$ when $0° < \alpha, \beta < 90°$ and $180° < \alpha, \beta < 270°$, and $\omega = \omega_q$ when $90° < \alpha, \beta < 180°$ and $270° < \alpha, \beta < 360°$.

containing the suspension are defined as parallel to the x, y, and z directions, respectively. The rotation angle of the capillary with respect to the x axis is denoted by angle α that changes over time as $\alpha = \omega t$. ω is ω_s when $0° < \alpha < 90°$ and $180° < \alpha < 270°$ and ω_q when $90° < \alpha < 180°$ and $270° < \alpha < 360°$ (Fig. 2).

With the rotation of the capillary, the microcrystals align three-dimensionally. This alignment is synchronous with the capillary rotation and is only maintained while the capillary rotation is continued. Because the speed of the conventional oscillation is much slower than that of the rotation, conventional measurement on the rotating capillary only reveals a fiber pattern. To collect the XRD images at a designated oscillation angle, we need to introduce a shutter device. The rotation angle of a disk-shaped shutter with respect to the y'-axis is denoted by $\beta = \omega t$; its rotation is synchronized with that of the capillary. There is a pair of slits, SL1 and SL2, with a slit angle of $\Delta\beta$, separated by 180° on the edge of the shutter. The angle $\Delta\beta$ corresponds to the widths of the ω-oscillation scan angle in conventional single-crystal measurement. The X-ray is allowed to impinge on the capillary only when the X-ray beam comes across the slits. Because a MOMS has a two-fold rotation symmetry about the capillary rotation axis,[22] the diffraction images taken through SL1 and SL2 are equivalent. The default starting position of the slits is at $\beta = 0$ when the capillary position is $\alpha = 0$ (see Fig. 1a). By shifting the starting position of the slits, the microcrystals are impinged by X-rays from different angles ω with respect to the X-ray beam. A set of collected diffraction data corresponds to that obtained from ω-oscillation scans in conventional single-crystal data acquisition. As a result, the obtained full data set can be analyzed by conventional computer software for single-crystal analyses.

Sample preparation of a suspension of L-alanine microcrystals, *in situ* X-ray measurement of the resulting MOMS, and subsequent single-crystal analyses are summarized in the ESI.† We used two kinds of suspensions, one containing 20–45 μm microcrystals and the other less than 5 μm (shown in Fig. 3). Single-crystal diffraction from microcrystals less than 10 μm in size is hard to measure using in-house diffractometers. It is even sometimes difficult to obtain single-crystal diffraction patterns from microcrystals with a size of 5 μm at conventional beam lines in synchrotron facilities. L-Alanine single crystals belong to the orthorhombic crystal system (space group: $P2_12_12_1$). The relationships between the
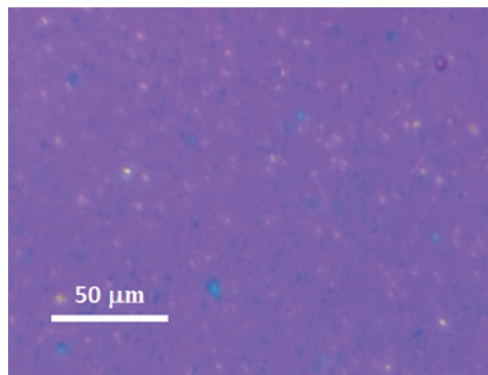
Fig. 3 Polarized optical micrograph of L-alanine microcrystals.

Fig. 5 X-ray diffraction patterns of an L-alanine MOMS (particle size: <5 mm) taken under (a) $30° < \alpha < 40°$ and (b) $80° < \alpha < 90°$.

magnetization and crystallographic axes for L-alanine crystals are known to be $\chi_1 \parallel c^*$, $\chi_2 \parallel a^*$, $\chi_3 \parallel b^*$.[24]

When a suspension is rotated about the z axis, the reciprocal b^* axis aligns parallel to the z axis, while the reciprocal a^* and c^* axes are in the xy plane, rotating in synchronization with the rotation of the suspending liquid medium.[21] Typical in situ diffraction images obtained for an L-alanine MOMS (20–45 μm) are presented in Fig. 4, where Fig. 4a–c are the diffraction images captured for $30° < \alpha < 40°$, $80° < \alpha < 90°$, and $140° < \alpha < 150°$, respectively. The diffraction spots are asymmetrically distributed about the capillary rotation axis (horizontal) and the three diffraction images exhibit different patterns. Fig. 4d is a diffraction image taken without the shutter. In this case, the diffraction spots are distributed symmetrically about the sample rotation axis (horizontal), which is similar to a fiber diffraction pattern. The diffraction images obtained for 5 μm microcrystals are shown in Fig. 5. Here the diffraction spots are broader than those for 20–45
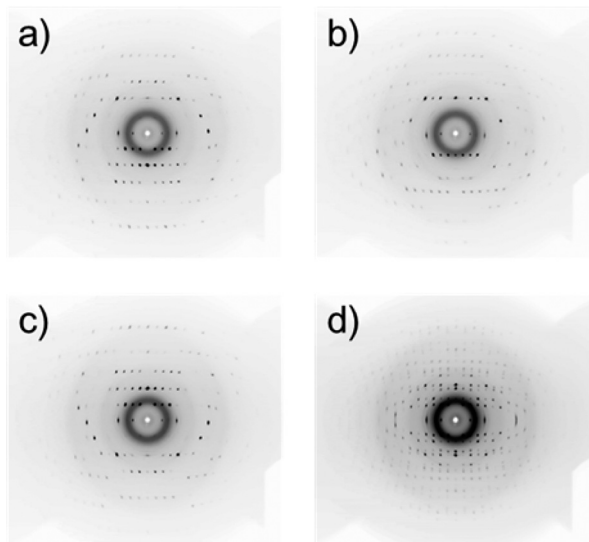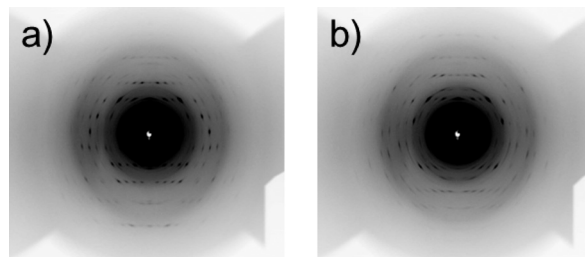
μm microcrystals because smaller microcrystals exhibit larger fluctuations in orientation. However, this quality of diffraction is sufficient for the subsequent analyses.

Crystallographic data determined using the MOMSs prepared from microcrystalline powders of 20–45 μm and <5 μm size are summarized in Table 1. They show good agreement with that reported in the literature.[25]

The data completeness for both samples was about 85%, which is not very high because the diffraction was only collected about the sample rotating axis parallel to the $\chi_3 \parallel b^*$ axis of L-alanine. By tilting the rotation axis of the capillary in the horizontal plane, the remaining XRD spots will be collected and the completeness will be increased. The structures determined are shown graphically in Fig. 6. Both of them are in good agreement with that determined from a single crystal reported in the literature.[25]

The crystal size limitation of this measurement can be estimated to be of submicron order as follows. The degree of orientation depends on the size of the microcrystals. Higher degrees of orientation can be achieved when the anisotropic magnetic energy markedly exceeds the thermal energy; that is, $(2\mu_0)^{-1} \chi_a V B^2 \gg k_B T$, where k_B is the Boltzmann constant, μ_0 is the magnetic permeability of vacuum, T is absolute temperature, V is the volume of the microcrystal, and χ_a is $\chi_1 - \chi_2$

Fig. 4 Polarized X-ray diffraction patterns of an L-alanine MOMS (particle size: 20–45 mm) taken at various angles of αs defined in Fig. 2, including (a) $30° < \alpha < 40$, (b) $80° < \alpha < 90°$, and (c) $140° < \alpha < 150°$. (d) A diffraction pattern taken without the shutter.

Table 1 Crystallographic data obtained from the MOMS and a single crystal

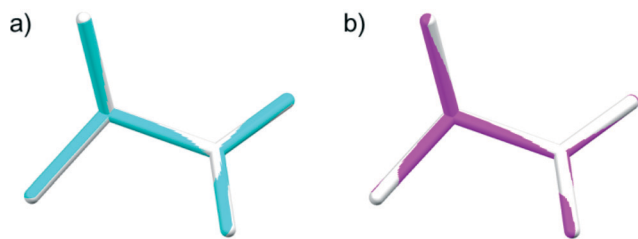| Sample	L-Alanine MOMS (20–45 μm)	L-Alanine MOMS (<5 μm)	L-Alanine[25] LALNIN53
Crystal system	Orthorhombic	Orthorhombic	Orthorhombic
Space group	$P2_12_12_1$	$P2_12_12_1$	$P2_12_12_1$
Temperature (K)	296	296	295(1)
a (Å)	6.031(2)	6.0350(17)	6.035(1)
b (Å)	12.318(4)	12.316(3)	12.361(3)
c (Å)	5.779(2)	5.7772	5.7762(9)
V (Å³)	429.3(3)	429.4(2)	430.86(1)
Z	4	4	4
$2\theta_{max}$	51.9(Mo $K\alpha$)	51.3(Mo $K\alpha$)	52.74(Mo $K\alpha$)
Independent reflections	3240(680)	3242(684)	3183(883)
Completeness	0.845	0.851	1.00
R_{int}	0.0315	0.0923	0.0427
$R_1 [F^2 > 2\sigma(F^2)]$	0.0421	0.0991	0.0378
wR [all data]	0.1012	0.3083	0.0736
GOF	1.106	1.060	1.044
CCDC no.	1055776	1429401	756484

Fig. 6 The structures determined by MOMS prepared from microcrystalline powders of a) 20–45 μm (blue) and b) <5 μm (pink) size are compared with the structure (white) reported previously.[25] The root-mean-square deviations are 0.0037 Å and 0.0130 Å for a) and b), respectively.

or $\chi_2 - \chi_3$, whichever is smaller. The larger the magnetic energy, the higher the degree of orientation. Inserting typical values of T = 300 K, B = 1T, χ_a = 10^{-7} (this value can be smaller or larger depending on the material), we obtain $V \gg 0.1$ μm^3, indicating that microcrystals of a few hundred nanometers in diameter can exhibit considerable orientation.

The crystallinity of the microcrystals also affects the degree of orientation through the value of χ_a. For example, if the mosaicity of the microcrystal is high, or a single particle is polycrystalline, χ_a becomes small, resulting in a low degree of orientation.

Conclusions

In this study, we demonstrated that single-crystal XRD analysis is possible from a microcrystalline powder by using an orientation attachment mounted on an in-house X-ray diffractometer. Single-crystal analysis of L-alanine microcrystals using this setup was performed, demonstrating that the determined crystal structure was in excellent agreement with that reported in the literature. This attachment allows the structure determination of microcrystals of 20 μm down to less than 5 μm in size only with in-house X-ray diffractometers, without a synchrotron X-ray source or the use of a powder diffraction method. This experimental circumstance will greatly facilitate the crystal structure determination required in various areas including chemistry, materials science, structural biology, pharmaceutics, *etc.*

Acknowledgements

Notes and references

1 L. Ooi, *Principles of X-ray Crystallography*, Oxford University Press, New York, 2010, pp. 112–122.

2 M. P. Blakeley, P. Langan, N. Niimura and A. Podjarny, *Curr. Opin. Struct. Biol.*, 2008, **18**, 593.

3 M. Adachi, T. Ohhara, K. Kurihara, T. Tamada, E. Honjo, N. Okazaki, S. Arai, Y. Shoyama, K. Kimura, H. Matsumura, S. Sugiyama, H. Adachi, K. Takano, Y. Mori, K. Hidaka, T. Kimura, Y. Hayashi, Y. Kiso and R. Kuroki, *Proc. Natl. Acad. Sci. U. S. A.*, 2009, **106**, 4641.

4 C. Giacovazzo, *Acta Crystallogr., Sect. A: Found. Crystallogr.*, 1996, **52**, 331.

5 Structure Determination from Powder Diffraction Data, *IUCr Monographs on Crystallography 13*, ed. W. I. F. David, K. Shankland, L. B. McCusker and C. Baerlocher, Oxford University Press, Oxford, 2002.

6 K. D. Harris and E. Y. Cheung, *Chem. Soc. Rev.*, 2004, **33**, 526.

7 G. Oszlányi and A. Süto, *Acta Crystallogr., Sect. A: Found. Crystallogr.*, 2008, **64**, 123.

8 W. I. F. David and K. Shankland, *Acta Crystallogr., Sect. A: Found. Crystallogr.*, 2008, **64**, 52.

9 K. Fujii, M. T. Young and K. D. M. Harris, *J. Struct. Biol.*, 2011, **174**, 461.

10 K. Shankland, M. J. Spillman, E. A. Kabova, D. S. Edgeley and N. Shankland, *Acta Crystallogr., Sect. C: Cryst. Struct. Commun.*, 2013, **69**, 1251.

11 A. Altomare, C. Cuocci, C. Giacovazzo, A. Moliterni, R. Rizzi, N. Corriero and A. Falcicchio, *J. Appl. Crystallogr.*, 2013, **46**, 1231.

12 P. A. Williams, C. E. Hughes and K. D. M. Harris, *Angew. Chem., Int. Ed.*, 2015, **54**, 3973.

13 W. Lasocha and H. Schenk, *J. Appl. Crystallogr.*, 1997, **30**, 561.

14 T. Wessels, C. Baerlocher and L. B. McCusker, *Science*, 1999, **284**, 477.

15 J. Grässlin, L. B. McCusker, C. Baerlocher, F. Gozzo, B. Schmitt and L. Lutterotti, *J. Appl. Crystallogr.*, 2013, **46**, 173.

16 T. Oda, K. Makino, I. Yamashita, K. Namba and Y. Maéda, *Biophys. J.*, 1998, **75**, 2672.

17 T. Oda, M. Iwasa, T. Aihara, Y. Maéda and A. Narita, *Nature*, 2009, **457**, 441.

18 J. Y. Genoud, M. Staines, A. Mawdsley, V. Manojlovic and W. Quinton, *Supercond. Sci. Technol.*, 1999, **12**, 663.

19 T. Kimura and M. Yoshino, *Langmuir*, 2005, **21**, 4805.

20 F. Kimura, W. Oshima, H. Matsumoto, H. Uekusa, K. Aburaya, M. Maeyama and T. Kimura, *CrystEngComm*, 2014, **16**, 6630. References therein.

21 M. J. Glucksman, R. D. Hay and L. Makowski, *Science*, 1986, **231**, 1273–1276.

22 N. Terada, H. S. Suzuki, T. S. Suzuki, H. Kitazawa, Y. Sakka, K. Kaneko and N. Metoki, *Appl. Phys. Lett.*, 2008, **92**, 112507.

23 K. Matsumoto, F. Kimura, S. Tsukui and T. Kimura, *Cryst. Growth Des.*, 2011, **11**, 945.

24 F. Kimura, T. Kimura, K. Matsumoto and N. Metoki, *Cryst. Growth Des.*, 2010, **10**, 48.

25 V. S. Minkov, Y. A. Chesalov and E. V. Boldyreva, *J. Struct. Chem.*, 2010, **51**, 1052. "CCDC Refcode: LALNIN53".